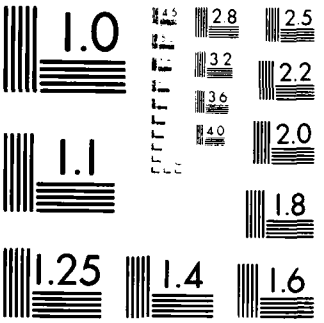

AFOSR-82-0298

Analysis of the Dissipationmechanism within an Instationary Cathode Spot of Metalvapor Arcs

H.O. Schrade, H.L. Kurtz, M. Auweter-Kurtz
and M. Kirschner

IRA

INSTITUT FÜR RAUMFAHRTANTRIEBE
UNIVERSITÄT STUTTGART

PFAFFENWALDRING 31
7000 STUTTGART 80 (VAIHINGEN)

(3)

AFOSR-82-0298

Analysis of the Dissipationmechanism within an Instationary Cathode Spot of Metalvapor Arcs

H.O. Schrade, H.L. Kurtz, M. Auweter-Kurtz
and M. Kirschner

IRA 84 IB-6

August 1984

Interim Scientific Report
Approved for public release; distribution unlimited

prepared for

Air Force Office of Scientific Research
Bolling AFB, D.C. 20332

and

European Office of Aerospace Research
and Development
London, England

UNCLASSIFIED

SECURITY CLASSIFICATION OF THIS PAGE (When Data Entered)

REPORT DOCUMENTATION PAGE	READ INSTRUCTIONS BEFORE COMPLETING FORM
1 REPORT NUMBER: AFOSR-TR- 84-1166	2 GOVT ACCESSION NO. / 3 RECIPIENT'S CATALOG NUMBER
4 TITLE and Subtitle: Analysis of the Dissipationmechanism within an Instationary Cathode Spot of Metalvapor Arcs	5 TYPE OF REPORT & PERIOD COVERED: ANNUAL 01.Aug.1983-31.July 1984
	6 PERFORMING ORG. REPORT NUMBER: IRA - 84 IB 6
7 AUTHOR(s): H.O. Schrade, H.L. Kurtz, M. Auweter-Kurtz and M. Kirschner	8 CONTRACT OR GRANT NUMBER(s): AFOSR-82-0298
9 PERFORMING ORGANIZATION NAME AND ADDRESS: Institut für Raumfahrtantriebe Universität Stuttgart, Pfaffenwaldring 31 7000 Stuttgart 80, West Germany	10 PROGRAM ELEMENT, PROJECT, TASK AREA & WORK UNIT NUMBERS: 61102F 2308/A1
11 CONTROLLING OFFICE NAME AND ADDRESS: AIR FORCE OFFICE OF SCIENTIFIC RESEARCH/NA BOLLING AFB DC 20332-6448	12 REPORT DATE: August 17, 1984
	13 NUMBER OF PAGES: 42
14 MONITORING AGENCY NAME & ADDRESS (if different from Controlling Office)	15 SECURITY CLASS. (of this report): Unclassified
	15a DECLASSIFICATION/DOWNGRADING SCHEDULE

16 DISTRIBUTION STATEMENT (of this Report)

Approved for public release; distribution unlimited.

17 DISTRIBUTION STATEMENT (of the abstract entered in Block 20, if different from Report)

18 SUPPLEMENTARY NOTES

None

19 KEY WORDS (Continue on reverse side if necessary and identify by block number)

Cathode spots, vapor pressure, energy dissipation mechanism, time dependent heat transfer.

20 ABSTRACT (Continue on reverse side if necessary and identify by block number)

The paper deals with the dissipation mechanism of microspots on low pressure arc cathodes.

Based on a new MPD stability theory and on an experimentally found empirical relation between spot current and crater radius on pure copper and molybdenum cathodes, the time behavior of pressure and

DD FORM 1 JAN 73 1473 EDITION OF 1 NOV 65 IS OBSOLETE

UNCLASSIFIED

SECURITY CLASSIFICATION OF THIS PAGE (When Data Entered)

temperature within the spot and the appertaining voltage drop have been calculated. Emphasis has been placed on finding an analytical solution for the time dependent heat flux into the hemispherical crater surface as a function of the expansion of the spot.

PREFACE

This report deals with the time dependent energy dissipation mechanisms which should occur in micro spots on cold metal cathode surfaces of low pressure arcs.

The Appendices A and B contain especially the mathematical way of how the analytical solution of the time dependent heat transfer equation and the formula for the time dependent heat flux for a growing spherical spot has been found.

This research has been sponsored in part by the Air Force Office of Scientific Research/US Air Force under Grant AFOSR 82-0298.

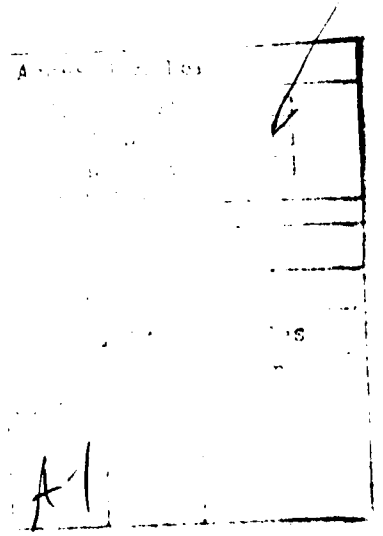

TABLE OF CONTENTS

ABSTRACT

The paper deals with the dissipation mechanism of microspots on low pressure arc cathodes.

Based on a new MPD stability theory and on an experimentally found empirical relation between spot current and crater radius on pure copper and molybdenum cathodes, the time behavior of pressure and temperature within the spot and the appertaining voltage drop have been calculated. Emphasis has been placed on finding an analytical solution for the time dependent heat flux into the hemispherical crater surface as a function of the expansion of the spot.

SURVEY OF PICTURES AND DIAGRAMS

LIST OF PARAMETERS

A_c	Surface of the melting within the crater
A_s	Phase boundary area solid/fluid within the crater
A_z	Cross section area of the channel within the plane of the cathode surface
$\vec{B}$	Magnetic induction
c	Evaporation constant
$C_1, C_2,$ C_3	Vapor pressure constants
C_f	Specific heat of the cathode material
$\vec{E}$	Intensity of electric field
$\vec{e}_c$	Unit vector
$\vec{e}_z$	Unit vector
f	Factor depending on current density distribution
$f(\tau)$	Function
h	Enthalpy
I	Current
$\vec{j}$	Current density
M	Molar mass
$\dot{m}$	Massflow
m_0	Mass of an atom
$\overleftrightarrow{P}$	Pressure tensor
$p_c=p_D$	Vapor pressure above the melting

p_z	Pressure within the area A_z
p	Ambient pressure
Q_s	Heat of fusion
Q_v	Heat of vaporization
$\vec{q}$	Heat flow
$\vec{q}_c$	Heat flow into the area A_c
$\vec{q}_f$	Heat flow out of the phase area A_s
$\vec{q}_s$	Heat flow out of the melt into the phase area A_s
R	Universal gas constant
r_s	Crater radius of the phase area A_s
r_{so}	Radius of a sphere
$\dot{r}_s$	Velocity of the phase area A_s
r_o	Crater radius of the phase area A_c
$\vec{S}$	Radiation
$\vec{S}_c$	Radiation into the melt
T	Temperature
T_c	Evaporation temperature = temperature of the gas within the crater straight above the melt
T_o	Temperature at the surface of the sphere with r_{so}
T_s	Melting temperature
T_∞, T^*	Cathode temperature at infinity
T^*, T_s^*	Substituted temperature
t	Time
U_k	Voltage drop at the cathode

U_{II}	Voltage drop in zone II
U_{III}	Voltage drop in zone III
V	Volume
$\vec{v}$	Velocity
$\vec{v}_c$	Exhaust velocity of cathode material on the crater surface
v_z	Velocity component in z-direction within the area A_z
x, x_1	Mathematical variables
y	Function
β, β_f	Matter constant of cathode material
$\gamma(x)$	Function
δ, δ_{crit}	Stability functions
λ_f	Heat conductivity of cathode material
μ_o	Magnetic permeability of free space
ν, ν_f	Thermo diffusion constant of cathode material
ρ	Density
ρ_c	Gas density above the area A_c
ρ_f	Density of cathode material
σ_f	Electrical conductivity of cathode material
τ	Time
φ	Potential function
$\Phi(x)$	Error function
Φ_e	Work function

INTRODUCTION

According to todays knowledge the attachment region of a low pressure arc or a so-called metal vapor arc consists of one or more bright "spots" of very high current-density (10^{12} A/m^2 and even higher). A vapor jet (containing even droplets) and a current-carrying plasmachannel emanate from each of these microspots. The discharge channel which electrically connects the cathode with the anode or with the main inter-electrode plasma region is therefore exposed to a very strong axial flow.

These microspots are highly nonstationary, they propagate and disappear and, depending on the electrode material (oxidized surface layer, surface chemistry), surface roughness, overall temperature, and type and pressure of gas, these microspots can cluster together to macrospots of different sizes with different erosion rates.

This report presents an analytical investigation of the instationary energy dissipation mechanisms within an individual microspot on a pure copper and molybdenum cathode. It is based on the knowledge of an experimentally found, empirical relation between spot current and spot size and assumes a strong enough axial flow in order to maintain a stable straight discharge channel.

HEMISPHERICAL CRATER MODEL

The following analysis considers a simplified model which, however, according to experimental findings [3],[4], is quite reasonable. At first the arc attachment region is divided into five different zones (Fig. 1).

Zone I is the current carrying plasma channel which electrically connects the low pressure plasma of the interelectrode space with the crater zone II. This latter zone contains a complex, turbulent mixture of evaporated material like atoms, ions and electrons under fairly high pressure. Adjacent to the high pressure zone II is the molten layer zone III, which is connected to the solid cathode zone IV through a hemispherical phase transition area. Zone V is the gas and vapor region outside the current carrying channel and is characterized by the fact that no, or only an insignificant, current density is present here.

Cathode material is evaporated out of the crater which forms a gas and vapor jet, causing an axial flow within the current carrying plasma channel (zone I) and a diverging flow in the non-, or only weakly, electrically conducting ambient zone V. As often observed in experiments,this jet can contain droplets which indicate that the surface of the melt within the crater is boiling and, as will be shown later,that due to an explosively increasing pressure in the crater (zone II), molten material is pressed and ejected out around the crater rim. The behavior is indicated by the protruding rims of the craters left on the surface of cold metal cathodes that have been struck by an arc.

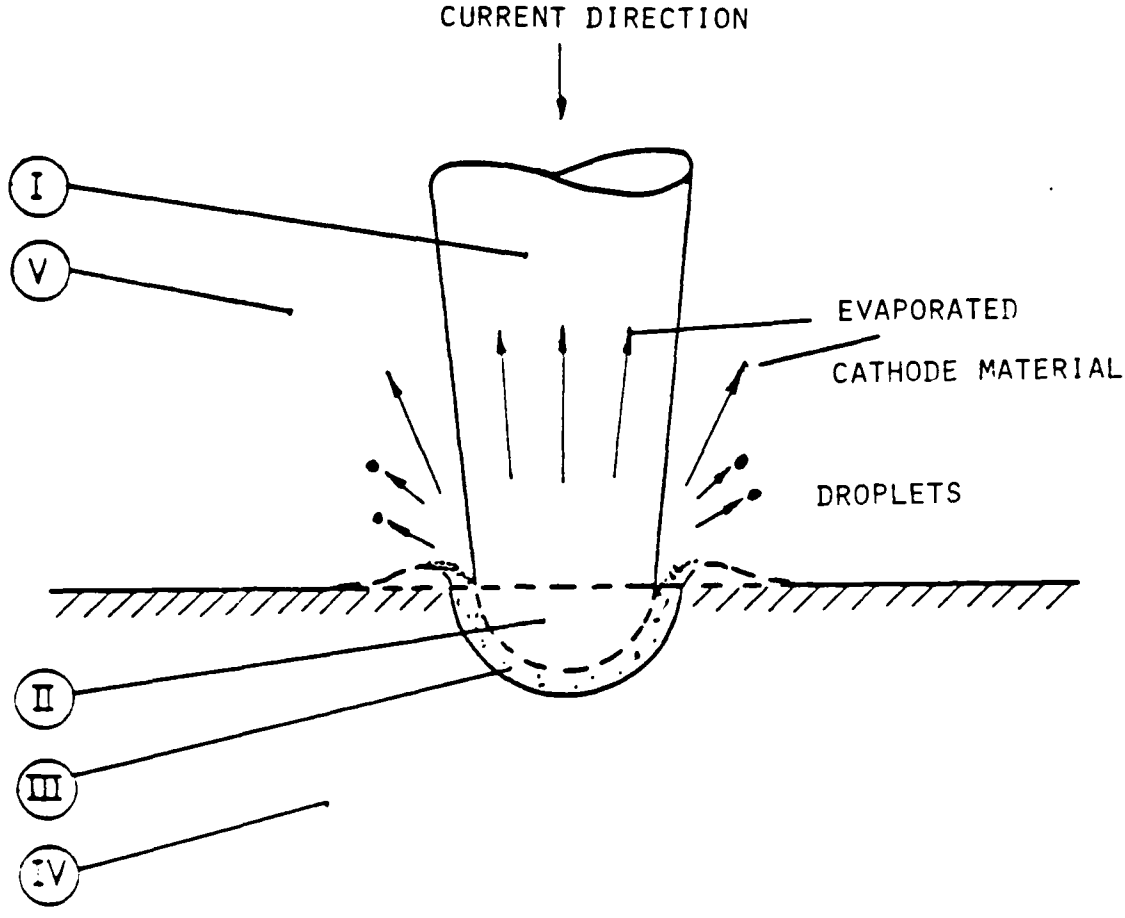

ZONE I	CURRENT CARRYING PLASMA CHANNEL
ZONE II	HEMISPHERICAL CRATER
ZONE III	MOLTEN METAL LAYER
ZONE IV	SOLID METAL CATHODE
ZONE V	NON CURRENT CARRYING GAS AND VAPOR REGION

Fig. 1: Hemispherical crater model

In our analysis we assume a hemispherical crater, neglecting this crater rim and the thrown out droplets. However, since these droplets have a minor effect on the energy balance, and since the crater radius follows as a function of the spot current from empirical relations of experimental observations, one indirectly accounts for the material loss due to this rim and droplet effect in zone III anyway.

ANALYSIS

Now we will investigate the zones separately and match the boundary conditions in between. Thus we obtain an integral view of the energy dissipation and at the same time the voltage drop U_K between the plasma channel (zone I) and the solid cathode (zone IV). It will be shown that this voltage drop fits very well with the cathode drop of a spotty arc discharge.

First we look at the current carrying plasma channel, zone I (Fig. 2). Former investigations in arc stability [5),6)] lead to the following criterion for a stable arc:

$$\varepsilon \equiv \int_{A_2} \rho v_z^2 \, dA_2 - \frac{\mu_0}{8\pi} I^2 [1+f] \geq \varepsilon_{krit} \qquad (1)$$

with

$$\varepsilon_{krit} \approx 0{,}1 \sqrt{A_2}\, I B_0 \qquad (2)$$

and $f \approx 0.8$

which means that the axial impulse transport within the discharge channel $\int_{A_2} \rho v_z^2 \, dA_2$ has to be larger than

$$\frac{\mu_0}{8\pi} I^2 [1+f] \left\{ 1 + 0{,}06 \cdot \frac{8\pi}{\mu_0} \frac{\sqrt{A_2}\, B_0}{I} \right\} \qquad (3)$$

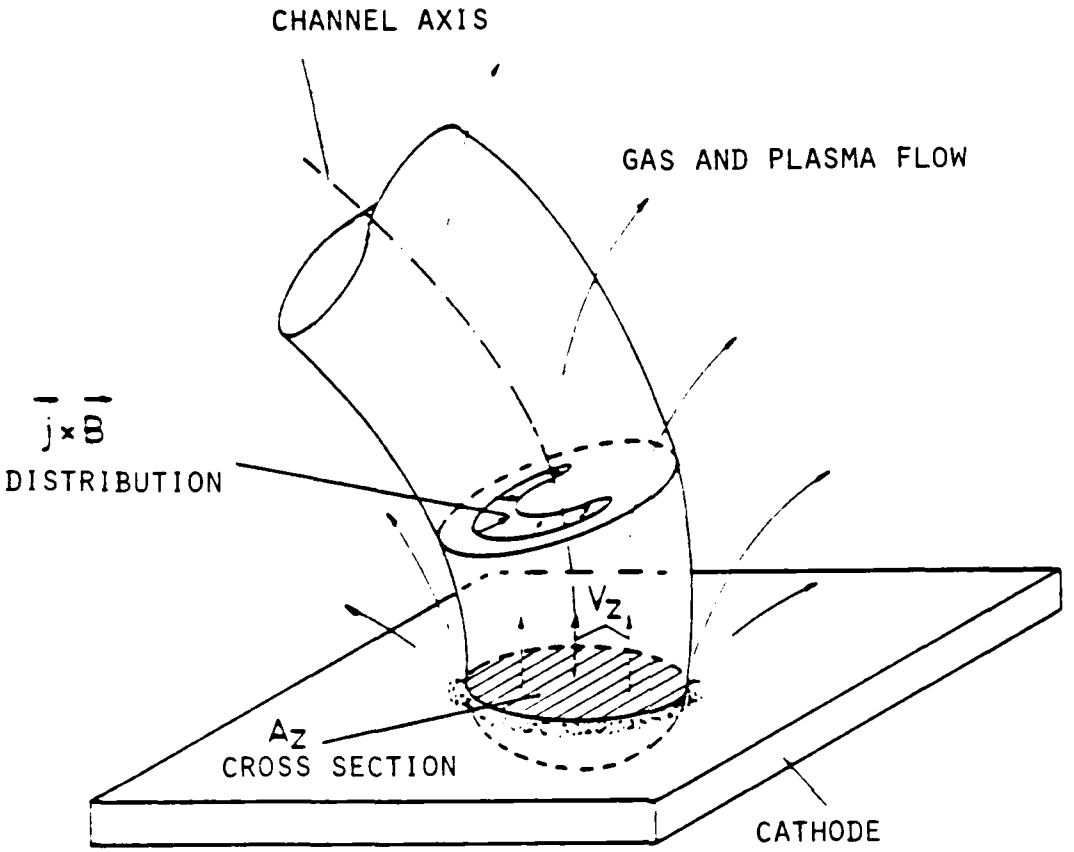

THE ELECTRICALLY CONDUCTIVE CHANNEL IS "KINK"-UNSTABLE AND BENDS MORE AND MORE IF:

$$\int_{A_z} \varrho \, v_z^2 \, dA_z < \frac{\mu_0}{8\pi} I^2 \left[1 + f \right]$$

WHERE $0.5 < f \leq 1$

AND $\varepsilon_{krit} \approx 0{,}1 \sqrt{A_z} \; I \, B_0$

Fig. 2: Zone I: current carrying plasma channel

For a pure copper cathode, we know from experiments [7] that $\sqrt{A_z}/I \approx 0.12$ (μm/A) . Using this we can neglect the second term within the curved brackets as long as the constant outer magnetic field is small enough ($B_0 \lesssim 1$ T) so the criterion above is reduced to $\varepsilon > 0$.

Utilizing the momentum equation for the crater zone II, the vapor pressure p_c above the molten layer can be related to the axial mass flow (Fig. 3). Neglecting the ambient pressure p , the criterion above can be expressed as

$$p_c \geq \frac{\mu_0}{8\pi} \frac{I^2}{A_z} \cdot 3{,}3 \qquad (4)$$

which means that in the case of our hemispherical crater model the vapor pressure above the melt has to be about 3 times the average magnetic pressure $p_M = \frac{\mu_0}{8\pi} \frac{I^2}{A_z}$.
If this condition does not hold, a small disturbance, which means a small curvature of the channel axis, will bend the channel more and more until it touches the electrode surface at another point and a new spot is created. Fig. 4 shows the vapor pressure curves for copper and molybdenum with another ordinate, the product of current and current density, Ij, with dimension A^2/cm^2. For Ij above these curves the current carrying plasma channel is unstable; correspondingly if Ij is less than the value given by these curves we have a stable discharge channel.
With the assumption that the mean evaporation rate from the fluid surface A_c within the crater corresponds to the vapor temperature T_c, which is the temperature of the gas within the crater straight above the melt and is

$$\dot{m} \approx A_c \rho_c \sqrt{\frac{k T_c}{2\pi m_0}} = A_c p_c \sqrt{\frac{m_0}{2\pi k T_c}} \qquad (5)$$

the criterion (4) becomes

$$\dot{m} \geq \frac{m_0}{8\pi} I^2 \sqrt{\frac{m_0}{2\pi k T_c}} \frac{A_c}{A_e} \cdot 3{,}3 = c \frac{\sqrt{M}\, I^2}{\sqrt{T_c}} \qquad (6)$$

with

$$c = 1{,}4 \cdot 10^{-9} \left[\frac{kg}{s} \frac{\sqrt{K}}{A^2} \right] \qquad (7)$$

M is the atomic or molecular mass of the evaporating cathode material.

The minimal evaporating rates for one spot at a pure copper and a pure molybdenum cathode yield to

$$\dot{m}_{Cu} = 3{,}5 \cdot 10^{-9} \frac{I^2}{\sqrt{T_c}} \left[\frac{kg}{s} \right] \qquad (6a)$$

$$\dot{m}_{Mo} = 4{,}3 \cdot 10^{-9} \frac{I^2}{\sqrt{T_c}} \left[\frac{kg}{s} \right] \qquad (6b)$$

with I in amperes and T in Kelvin.

These results are now used for the analysis of the dissipation mechanism together with the justified assumption that the voltage fraction of the spot is just high enough to obtain a stable spot.

First the energy equation for the crater zone II is formulated, which means that the power converted within zone II given by the electrical power input

$$\int_{V_{II}} \vec{E} \cdot \vec{j}\, dV = U_{II}\, I$$

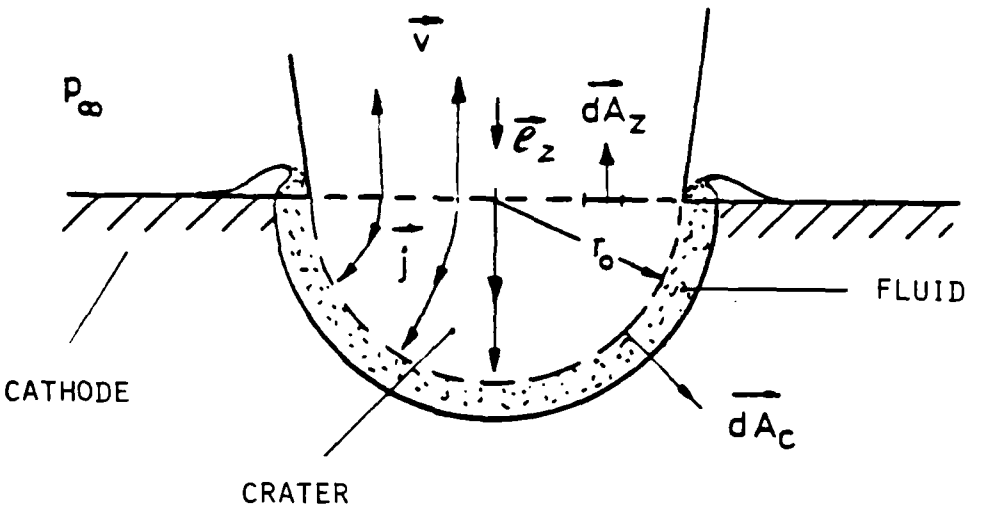

FORCE BALANCE:

$$\oint_A \{\rho \vec{v}\vec{v} + \vec{P}\} \cdot d\vec{A} = \int_V \vec{j} \times \vec{B}\, dV$$

$\vec{e}_z$ = UNIT VECTOR

$$-\int_{A_z} (\rho v_z^2 + p_z)\, dA_z + \int_{A_c} p_c\, d\vec{A}_c \cdot \vec{e}_z = \int_V \vec{j} \times \vec{B}\, dv \cdot \vec{e}_z$$

p_c AND $[\vec{j}]$ ARE HOMOGENEOUS ON THE INNER SURFACE OF THE CRATER

$$d\vec{A}_c \cdot \vec{e}_c = dA_z \quad : \quad \int_V \vec{j} \times \vec{B}\, dv \cdot \vec{e}_z = \frac{\mu_o}{8\pi} I^2 \{f - 0.2274\}$$

$$\int_{A_z} \rho v_z^2\, dA_z = \int (p_c - p_z)\, dA_z - \frac{\mu_o}{8\pi} I^2 \{f - 0.2274\}$$

STABILITY CRITERION:

$$p_c > p_\infty + \frac{\mu_o}{4\pi} \frac{I^2}{\pi r_o^2} \{1 + f - 0.1137\}$$

Fig. 3: Zone II: hemispherical crater

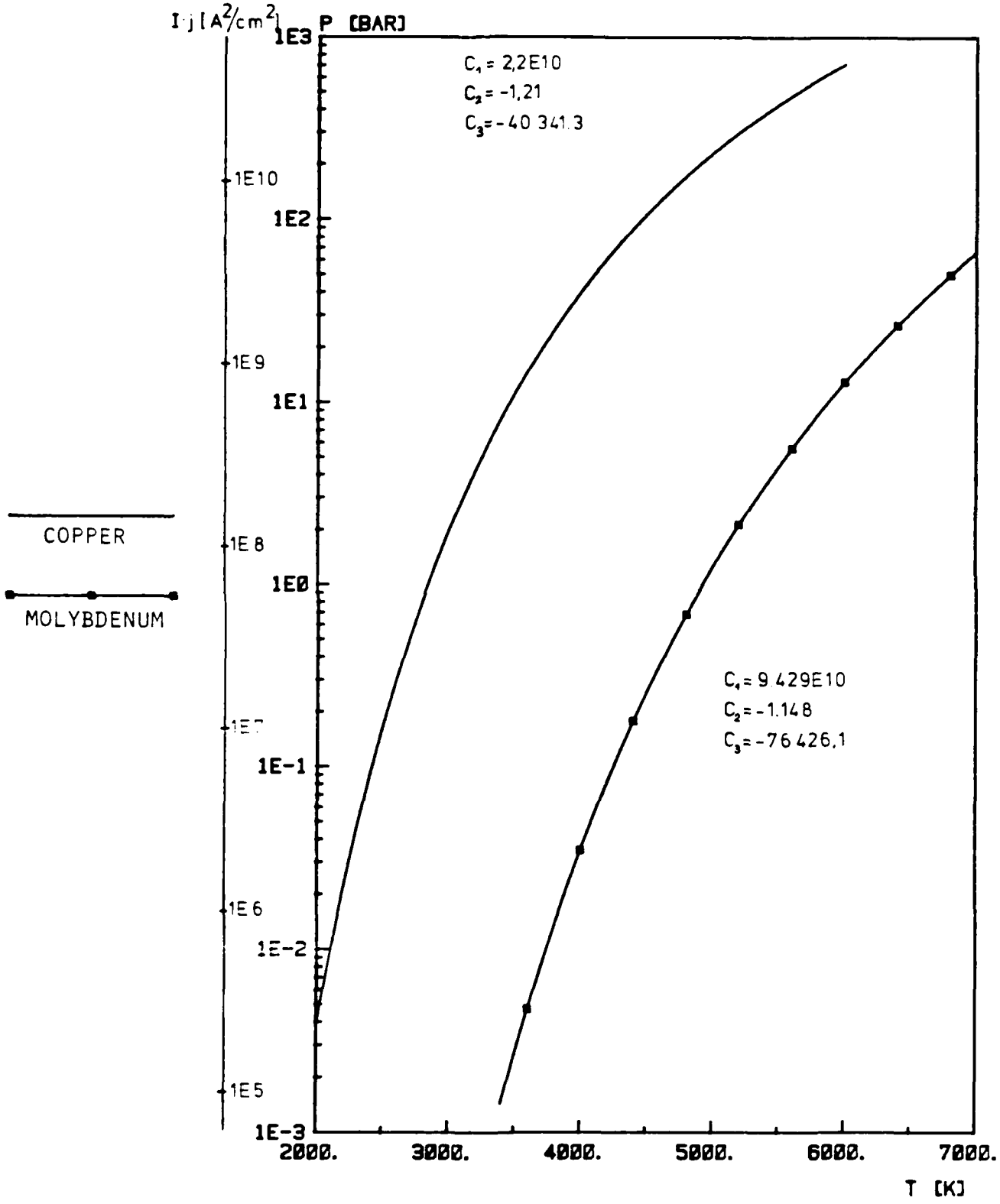

Fig. 4: vapor pressure curves for copper and molybdenum

$$P_c = C_1 \cdot T^{C_2} \cdot e^{(C_3/T)}$$

according to [10] and extrapolated for pressures above 1 bar

must be equal to the difference of energy which leaves and which enters the crater zone per unit time.

Within this calculation the purely convective part

$$\oint_{A_c+A_z} \varrho h \vec{v} \cdot d\vec{A}$$

and the parts due to heat transfer and radiation have to be separated. The convective energy flow can be expressed as $\dot{m} \Delta h$, where $\dot{m}$ is the evaporated mass through the crater area A_c. Because of the continuity equation, $\dot{m}$ is equal to the massflow through the circular crater orifice area A_z. Δh is the enthalpy difference of the plasma-vapor mixture between the orifice area A_z and the region directly above the melting zone III. Because the mean pressure and temperature at both areas are known, this enthalpy difference can be calculated. In this evaluation the resultant heat conduction and radiation loss through the area A_z can be neglected with respect to the convective effects. The radiation and heat transfers (which include ion bombardment) through the area A_c, however, contribute importantly to the heating up of the melting zone and to the evaporation of the cathode material.

The energy balance of zone III can be written in a similar way. The electrical energy ($I U_{III}$) within this zone equals the difference of outflowing and inflowing energy per second.

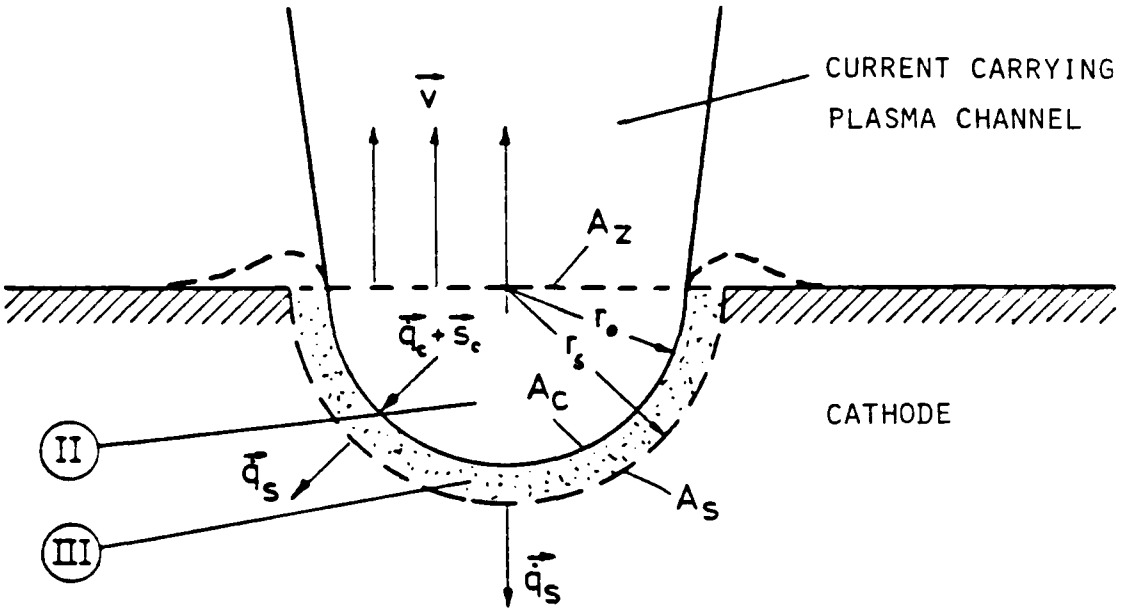

ENERGY BALANCE II:

$$\oint_{A_c+A_z} \varrho h (\vec{v} \cdot d\vec{A}) + \oint_{A_c+A_z} (\vec{q} + \vec{s}) \cdot d\vec{A} = \int_{V} \vec{E} \cdot \vec{j} \, dV$$

$$\dot{m} \, \Delta h + 2\pi r_0^2 (\dot{q}_c + s_c) = I \, U_{II} \; ; \quad \dot{m} = \int_{A_z} \varrho \, \vec{v} \cdot d\vec{A}_z$$

ENERGY BALANCE III:

$$\dot{m} \, Q_{verd} + I \, \phi_e + 2\pi r_s^2 \, \dot{q}_s - 2\pi r_0^2 (\dot{q}_c + s_c) = I \, U_{III}$$

SUM II AND III:

$$U_{II} + U_{III} = U_k$$

$$\boxed{\dot{m} \, (Q_v + \Delta h) + I \, \phi_e + 2\pi r_s^2 \, \dot{q}_s = I \, U_k}$$

Fig. 5: Zone II and III: crater and molten layer

Two other terms have to be added in the energy balance of zone III: $\dot{m}Q_v$ because of the transition of evaporated material to zone II, and $I\,\Phi_e$ because of the work function of the emerging electrons (Fig. 5). The energy of the particles which flow over the crater rim and that of the ejected droplets are neglected. It is a main fraction in respect to the mass but a minor fraction in respect to the energy in this zone.

The energy balance of the spotty cathode voltage drop is the sum of the voltage drops of the crater zone II and the liquid zone III (Fig. 5). This yields to

$$\dot{m}\,(Q_v + \Delta h) + I\,\phi_e + 2\pi r_s^2 \dot{q}_s = I\,U_K \qquad (9)$$

where $(2\pi r_s^2 \dot{q}_s)$ is the energy flow per second through the phase area solid-fluid because of heat conduction.
The evaporated mass $\dot{m}$ cannot become larger than the molten mass in the same time period; this leads to the requirement:

$$\dot{m} \leq 2\pi r_s^2 \dot{r}_s \rho_f \qquad (10)$$

From Fig. 6 the energy which causes the melting of the solid material can be calculated to

$$2\pi r_s^2 \dot{r}_s \rho_f Q_s = 2\pi r_s^2 (\dot{q}_s - \dot{q}_f) \qquad (11)$$

where Q_s is the heat of fusion and $\dot{q}_f$ the radial heat flow directed from the phase area liquid-solid to the solid zone IV.

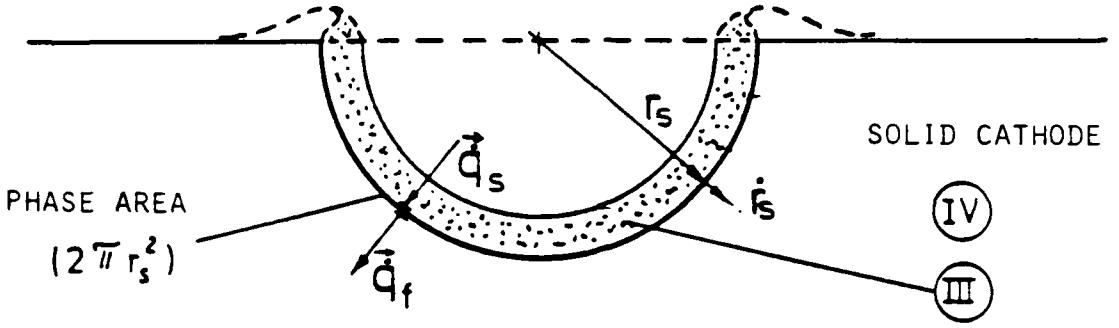

REQUEST: $$\dot{m} \leq 2\pi r_s^2 \dot{r}_s \rho_f = 2\pi r_s^2 \frac{\dot{q}_s - \dot{q}_f}{Q_s}$$

$$\boxed{2\pi r_s^2 \dot{q}_s \geq 2\pi r_s^2 \dot{q}_f + \dot{m} Q_s}$$

INTO THE ENERGY EQUATION

$$I U_\kappa \geq \dot{m} (\Delta h + Q_v + Q_s) + I \dot{\phi}_e + 2\pi r_s^2 \dot{q}_f$$

$$\boxed{U_\kappa \geq \frac{\dot{m}}{I} (\Delta h + Q_v + Q_s) + \dot{\phi}_e + 2\pi r_s^2 \frac{\dot{q}_f}{I}}$$

Fig. 6: Zone III and IV: phase area fluid-solid

With Eqs. (10) and (11) and the results from Fig. 5, the heat flow in the liquid zone can be expressed with respect to the heat flow in the solid zone. Therefore the cathode voltage drop follows as:

$$U_K = \frac{\dot{m}}{I}\left(\Delta h + Q_v\right) + \phi_e + \frac{2\pi r_s^2}{I}\left(\dot{r}_s \rho_f Q_s + \dot{q}_f\right) \qquad (12)$$

Before looking at the heat conduction $\dot{q}_f$ within the solid zone IV, the limitation of $\dot{m}$ caused by the stability criterion (6) and the above requirement (10) will be added. On a cold solid metal cathode the evaporation rate $\dot{m}$ within a spot is limited by

$$c\,\frac{\sqrt{M}\,I^2}{\sqrt{T_c}} \leq \dot{m} \leq 2\pi r_s^2 \dot{r}_s \rho_f = 2\pi r_s^2 \frac{\dot{q}_s - \dot{q}_f}{Q_s} \qquad (13)$$

To calculate the heat flow $\dot{q}_f$, the heat flow equation within zone IV (Fig. 7) has to be solved. Therefore two assumptions are made:

a) the heat transfer coefficient λ_f respectively the thermal diffusion coefficient χ_f within the solid is constant and

b) the term $\beta_f j^2$, which takes the ohmic heating within the solid into account, can be approximated step by step by a potential function with $\varphi \sim 1/r$.

Hence it is

$$\beta_f j^2 \simeq \varphi(r,t) \qquad (14)$$

with

$$\Delta\varphi = \frac{1}{r^2}\frac{\partial}{\partial r}\left(r^2 \frac{\partial}{\partial r}\varphi\right) = 0 \qquad (15)$$

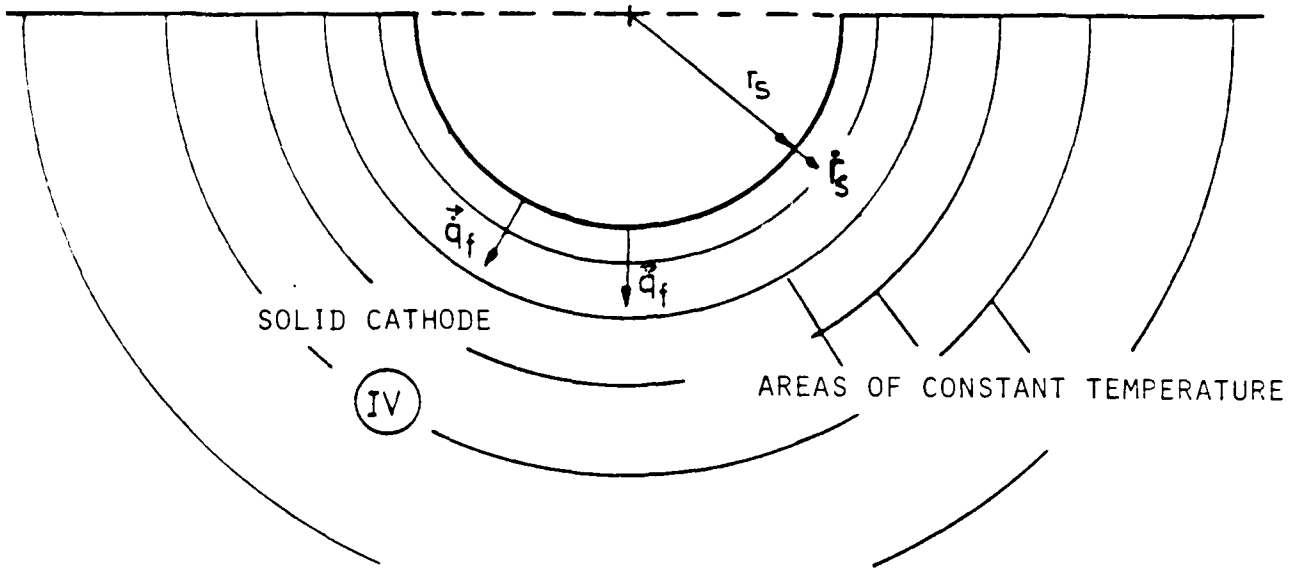

HEAT CONDUCTION EQUATION OF ZONE IV:

$$\frac{\partial}{\partial t} T = \frac{\chi_f}{r^2} \frac{\partial}{\partial r} \left(r^2 \frac{\partial}{\partial r} T \right) + \beta_f j^2$$

$$\chi_f = \frac{\lambda_f}{\rho_f c_f} = \text{CONST.}; \quad \beta_f = \frac{1}{\rho_f c_f \vartheta_f}; \quad j(r) = \frac{I}{2\pi r^2}$$

INITIAL CONDITIONS:

$$t = 0 \curvearrowright r_s(t=0) \equiv r_{so}, \quad r_s(t) = r_{so} + \int_0^t \dot{r}_s \, dt$$

BOUNDARY CONDITIONS:

$$r = r_s(t) \curvearrowright T(r_s, t) = T_s = \text{CONST.}$$

$$r \to \infty \curvearrowright T(r \to \infty, t) = T_\infty = \text{CONST.}$$

Fig. 7: Zone IV: solid metal cathode

in the region	the potential function is given as
$r_{s0} < r \leq r_1$	$\varphi(r,t) = \varphi_1(r,t)$
$r_1 < r \leq r_2$	$\varphi(r,t) = \varphi_2(r,t)$
$\vdots \quad \vdots$	$\vdots \quad \vdots$
$r_{\nu-1} < r \leq r_\nu$	$\varphi(r,t) = \varphi_\nu(r,t)$
$\vdots \quad \vdots$	$\vdots \quad \vdots$

Setting $\beta_f = \frac{1}{\rho_f \sigma_f c_f} = \text{const.}$, there follows because of $j = \frac{I}{2\pi r^2}$

$$\beta_f j^2 = \beta_f \frac{I^2}{4\pi^2} \frac{1}{r^4} \tag{16}$$

which is in fact no potential function. But within a small region $r_{\nu-1} < r \leq r_\nu$ the term (14) can be approximated by

$$\beta_f j^2 \cong \varphi_\nu = \beta_f \frac{I^2}{4\pi^2} \left(\frac{2}{r_\nu + r_{\nu-1}}\right)^3 \frac{1}{r}$$

where $\Delta \varphi_\nu = 0$ is nearly realized. This can be done within all regions $\nu = 1,2,3\ldots$. With this step by step approximation of $\beta_f j^2$ by a potential function φ the heat flow equation can be rearranged.
Replacing T by

$$T = T^* + \int_0^t \beta_f j^2 \, dt \tag{17}$$

where T* is the new independent variable
the new differential equation follows as

$$\frac{\partial}{\partial T} T^* = \frac{\chi_f}{r^2} \frac{\partial}{\partial r} \left(r^2 \frac{\partial}{\partial r} T^*\right) \tag{18}$$

SOLUTION : $T = T(r,t)$ IN THE RANGE : $t > 0$;

$r_s \leq r \leq \infty$

$$T - T_\infty = \frac{r_{s_o}}{r}(T_s - T_\infty)\left\{1 - \Phi(x) + \left[\frac{\int_o^t \dot{r}_s\,dt}{r_{s_o}} + \Phi(x_1)\right]\frac{\delta(x)}{\delta(x_1)}\right\} + \int_0^t \beta_f j^2\,dt$$

$$x = \frac{r - r_{s_o}}{2\sqrt{\chi_f t}} \quad ; \quad x_1 = \frac{\int_o^t \dot{r}_s\,dt}{2\sqrt{\chi_f t}} = \frac{r_s - r_{s_o}}{2\sqrt{\chi_f t}}$$

$$\Phi(x) = \frac{2}{\sqrt{\pi}}\int_0^x e^{-x^2}\,dx$$

$$\delta(x) = \left\{1 - \Phi(x)\right\}\cdot\left[1 + 2x^2\right] - \frac{2}{\sqrt{\pi}}\,x\,e^{-x^2}$$

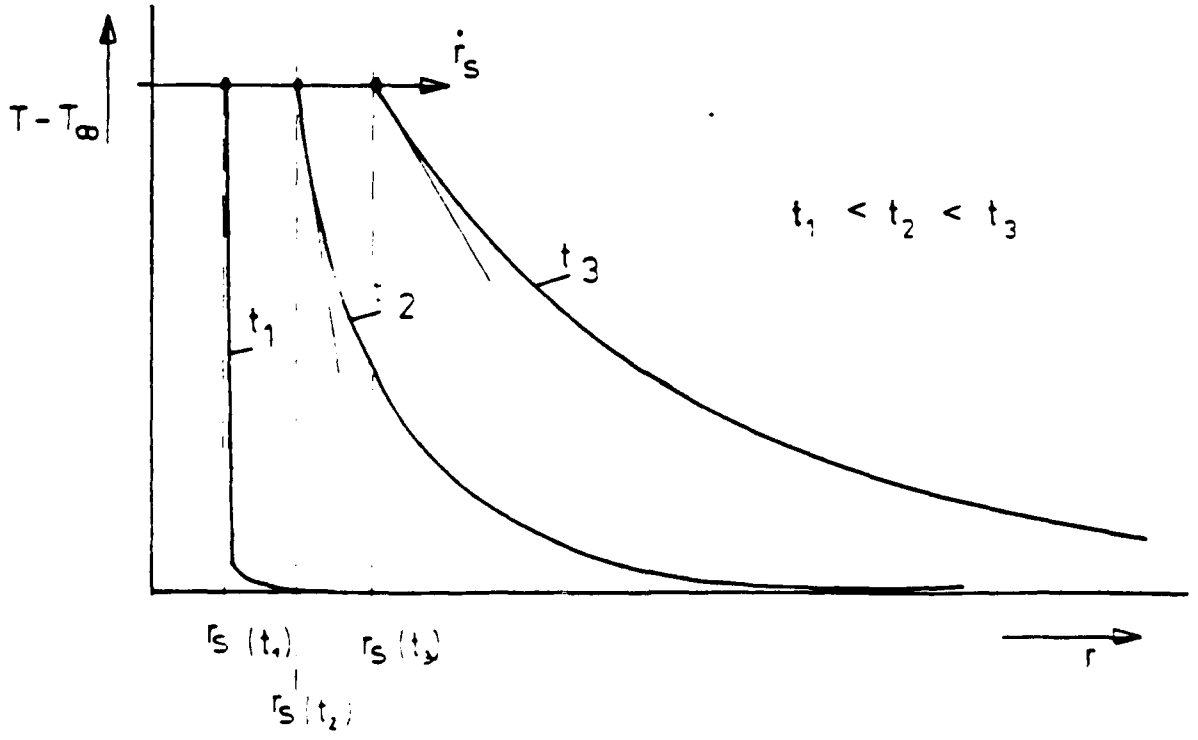

Fig. 8: Temperature distribution

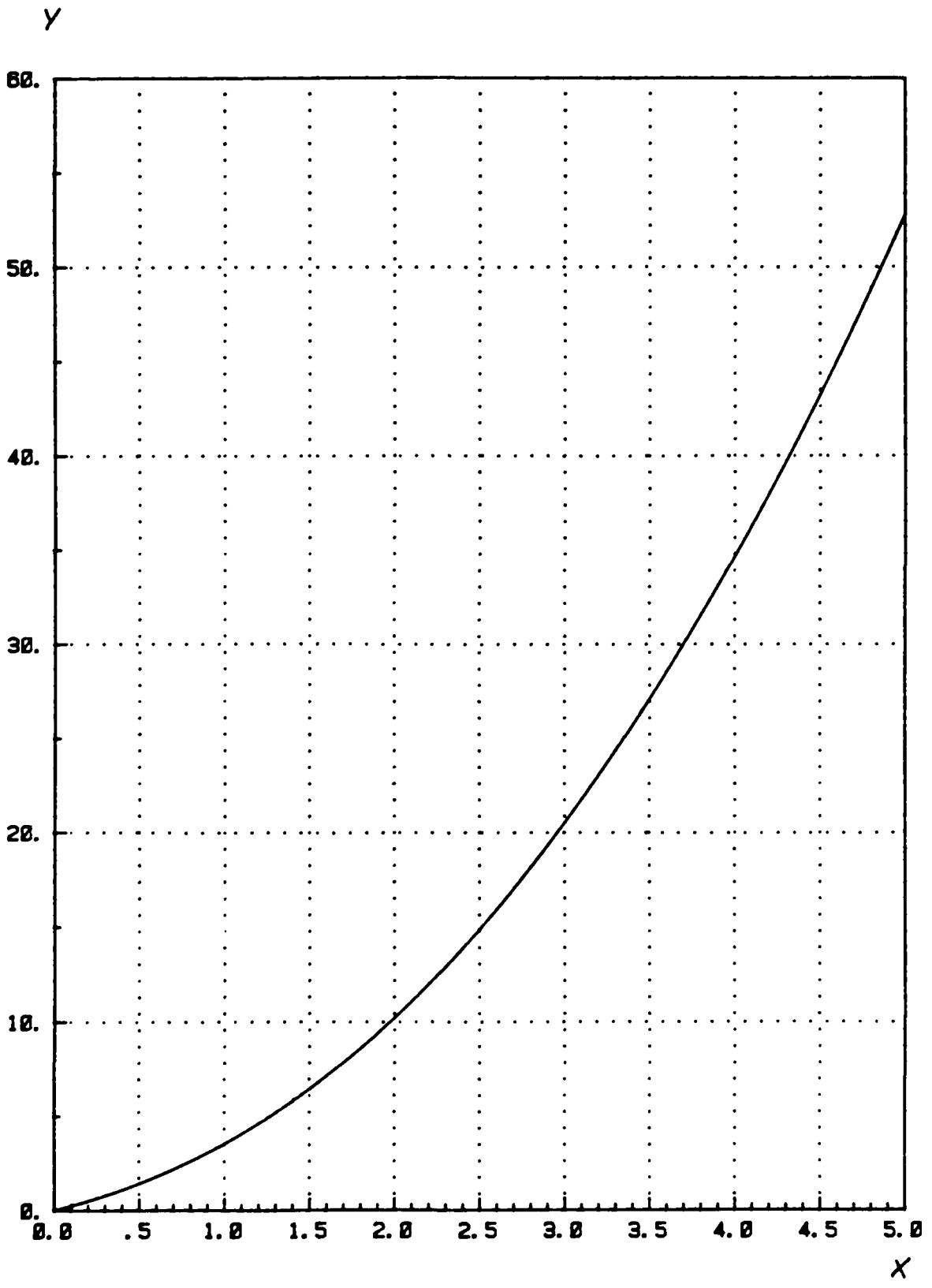

Fig. 9: Function $y = 2\left\{\frac{1-\Phi(x)}{\delta(x)} - 1\right\}$

which is solved for the given initial and boundary conditions in Appendix A. Equation (17) leads to the solution for the temperature T(r,t) which is shown in Fig. 8. Using this solution T(r,t) the heat conduction loss can be calculated by forming suitable gradients on the solid side of the phase area fluid-solid ($r=r_s$; exactly: $r=\lim_{\Delta r\to 0}(r_s+\Delta r)$).

In Appendix B the heat flow into the solid zone IV is calculated taking care of the fact that at time t=0 the initial radius is $r_{so}=0$;

$$2\pi r_s^2 \dot{q}_f(t) = 2\pi r_s \lambda (T_s - T_\infty)\left\{\left[1 + 2\left(\frac{1-\phi(x_s)}{\delta(x_s)} - 1\right)\right]\cdot \left[1 - \frac{\int_0^t \beta j_s^2 dt}{T_s - T_\infty}\right]\right\} \quad (19)$$

with $x_s = \frac{r_s(t)}{2\sqrt{\kappa t}}$.

The function $2\left(\frac{1-\phi(x_s)}{\delta(x_s)} - 1\right)$ is displayed in Fig. 9. Taking the rises of current I(t) and spot radius $r_s(t)$ from experiments [2] Eqs. (19) allows the calculation of the time dependent heat flow into the solid electrode. With this it is possible to determine the cathode drop voltage U_k (without inductive part), the minimal vapor pressure p_c and the spot temperature T_c as a function of time using Eqs. (12),(4) and vapor pressure diagrams (Fig. 4).

RESULTS AND DISCUSSION

It is known from experimental investigations 1),2),11) that during the first 3 to 5 ns of a pulsed discharge with a current rise of about 1 to $5 \cdot 10^9$ A/s, a small circular melting point occurs on the pure metal electrodes which afterwards forms a crater; then the crater rim expands with a velocity of 10^4 to $5 \cdot 10^4$ cm/s. After about 5 to 40 ns the final crater size is reached which means that the current transportation is incured by a new spot.

On pure metal cathodes the crater radius r_s increases with the current I_s. Experiments lead to the empirical approach:

$$r_s = r_o \, e^{I_s/I^*} \qquad (20)$$

with pure copper: $r_o = 1{,}7$ µm and $I^* = 83$ A
with pure molybdenum: $r_o = 1.2$ µm and $I^* = 33$ A [2].
It is now possible to analyze the time behavior of the dissipation mechanism of a cathode spot and to calculate the purely ohmic part of the cathode voltage as a function of time if one takes the spot current I_s as a given quantity which linearly rises with time.

Figures 10 and 11 show the results of these calculations for copper and molybdenum. In both cases the characteristic traces of the curves are similar to each other for the vapor pressure p_c, the surface temperature T_c and for the ohmic part of the voltage U_k.

During the initial phase the pressure rises explosively and sooner or later, depending on electrode material and current rise (dI/dt), it reaches a maximum. With copper

($dI/dT = 2.67\ 10^9$ A/s) this maximum of about 160 bar is reached after about 30 ns; with molybdenum ($dI/dt = 8 \cdot 10^9$ A/s) it needs only about 3.7 ns to get to the maximum of about 55 bar. This very significant, explosive pressure rise on the inner crater surface gives an explanation for the fluid metal which is ejected and which forms a crown like rim.

Initially the temperature rises steeply, later on it rises more slowly up to nearly 5000 K for copper, and nearly 7000 K for molybdenum. Nevertheless the temperatures do not reach the value which would be needed for a pure thermionic emission even in the case of molybdenum.

To explain the very high electron emission on the cathode G. Ecker postulated a combination of thermionic and field emissions [12]. This seems to be possible because new experiments [13] show field amplifying "Taylor cones" at formerly plane fluid surfaces. With this explanation the emission of the charged particles is not uniformly distributed on the inner fluid crater surface but will occur at one or more "Taylor cones" which emerge and vanish at the fluid surface. Therefore only the time average of the emission is uniform over the inner crater surface.

A complex, turbulent high pressure plasma exists in the crater-zone where the Debye-length reaches quite possibly only 10^{-8} to 10^{-7}m and therefore the electrical field at the tips of the "Taylor cones" could be some 10^9 V/m. With that, the relatively high emissions of 10^8 A/cm^2 (and more) can be explained. A further possibility would be the evaporation of negative ions out of the tip of such Taylor cones, similar to those observed with positive ions

Fig. 10: Spot behavior (cold, pure copper cathode)

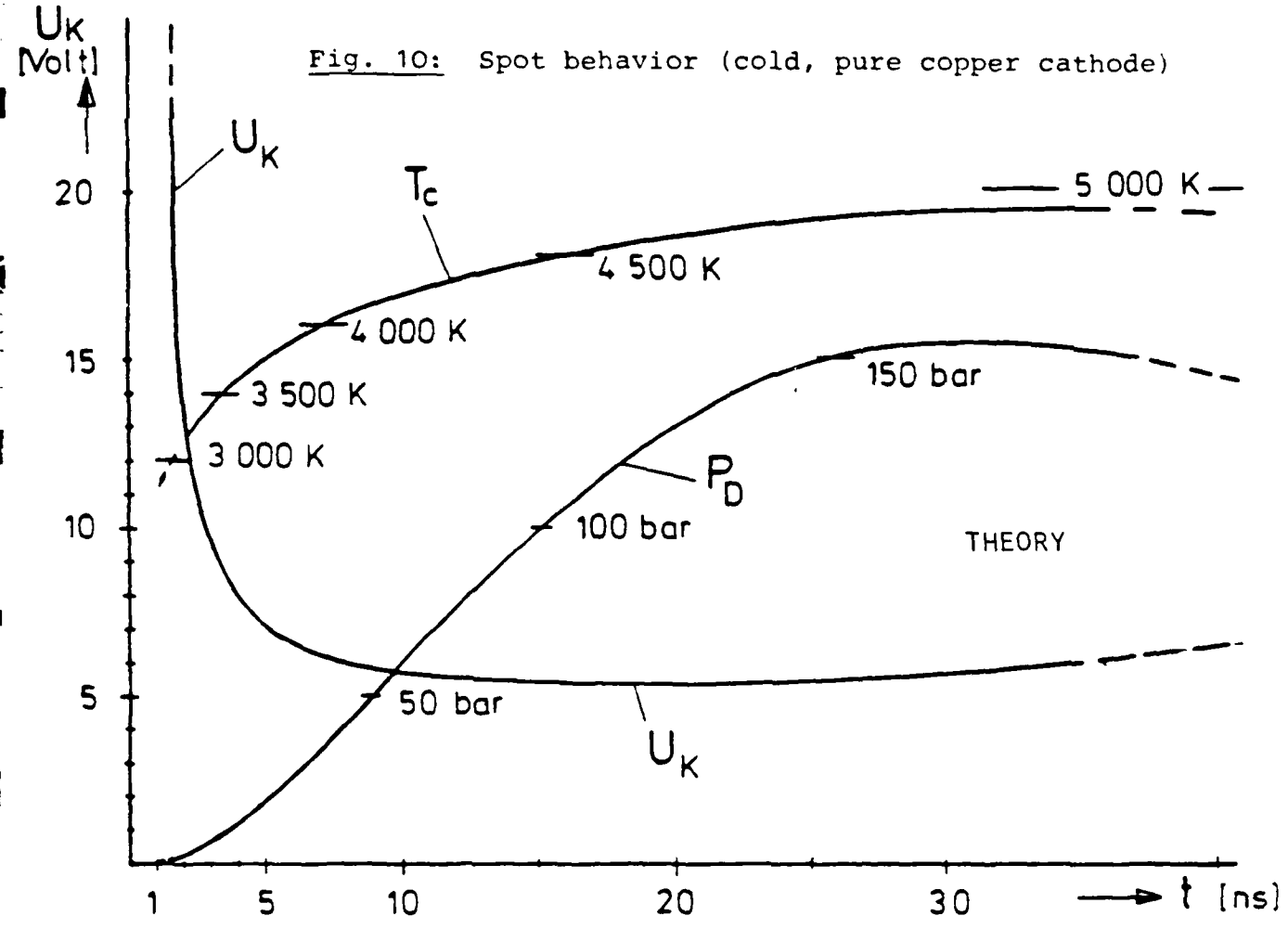

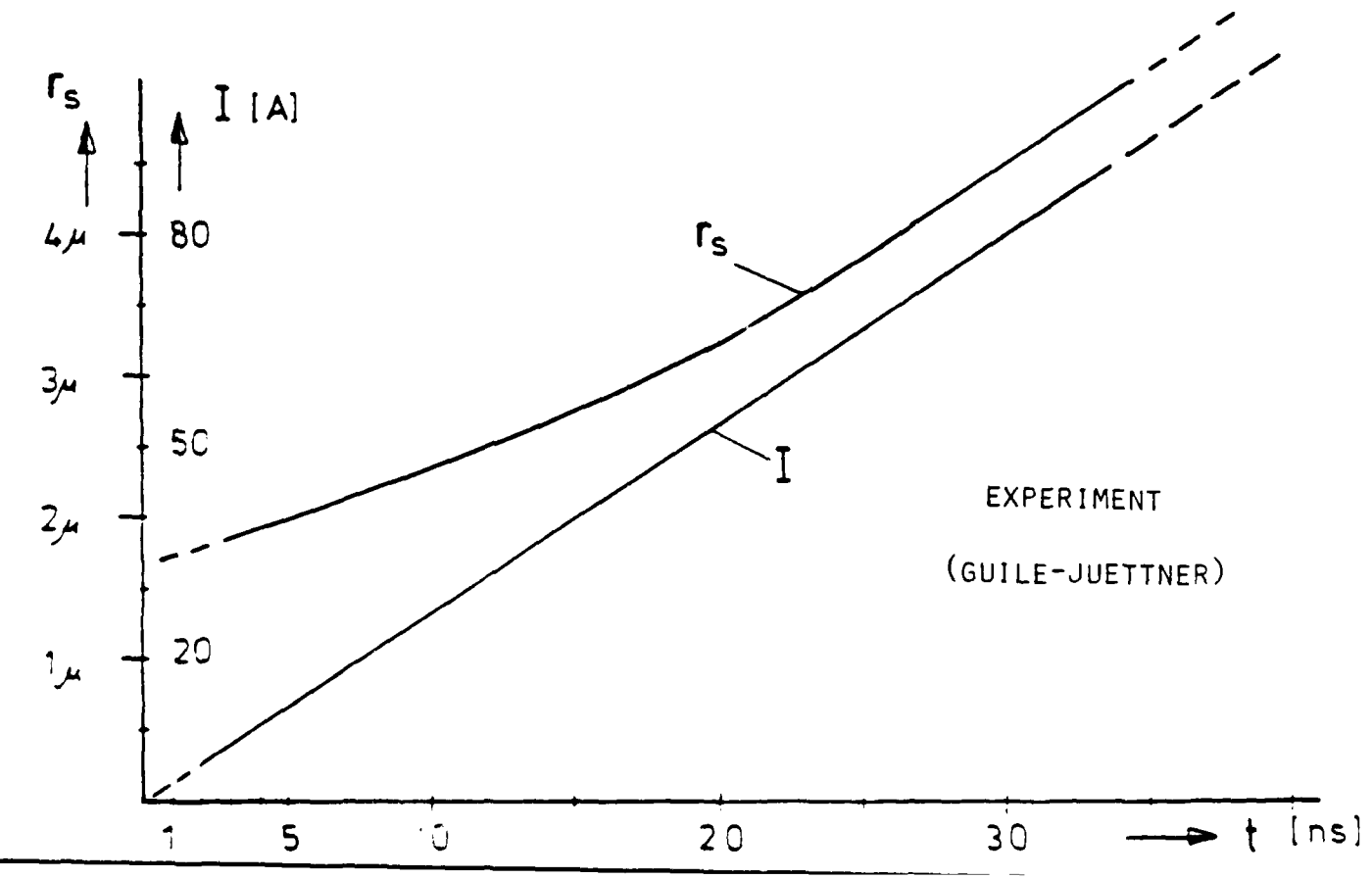

Fig. 11: Spot behavior (cold, pure molybdenum cathode)

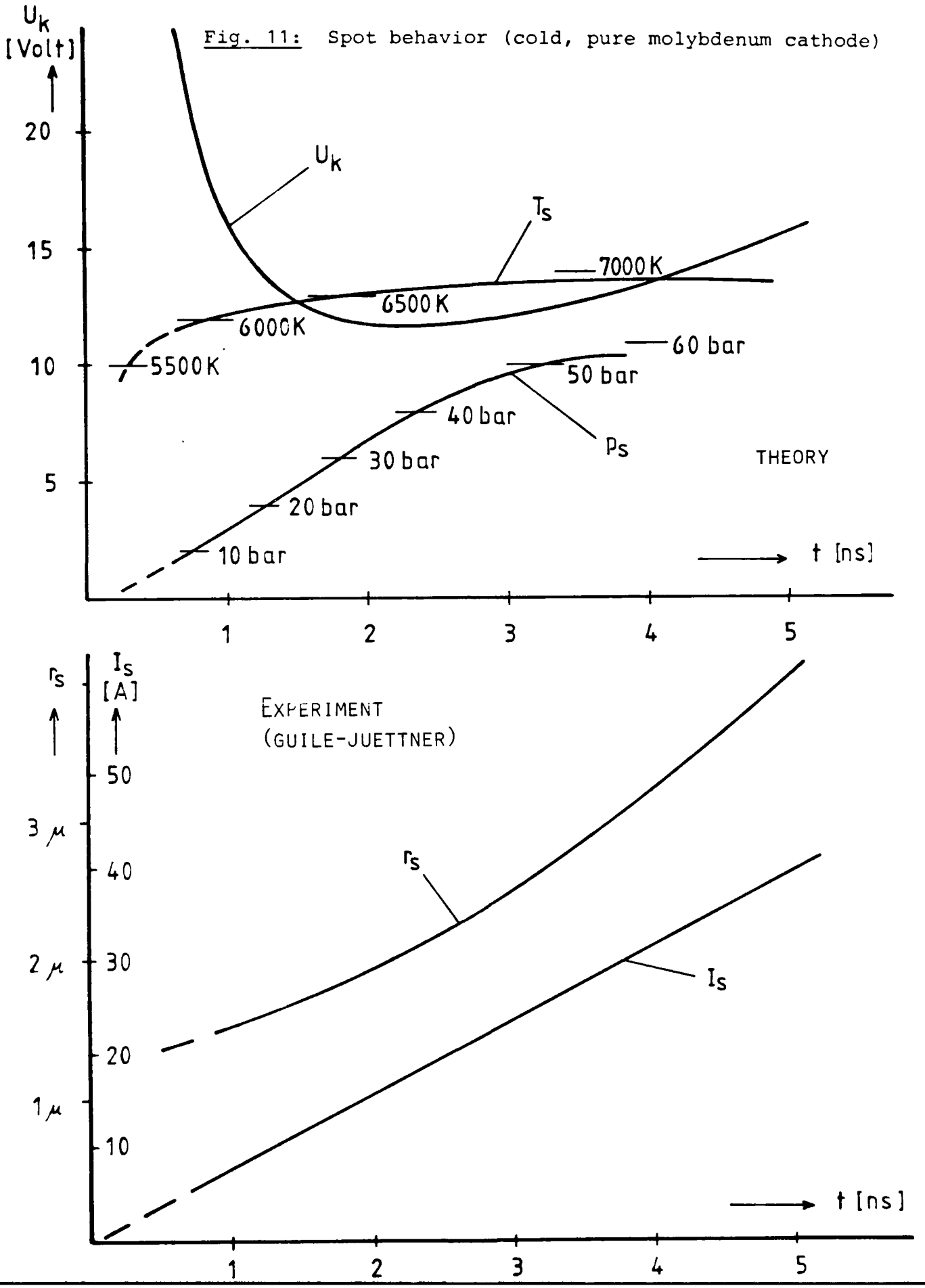

on anode tips [14],[15]. The life span of such negative ions within the crater plasma is expected to be short; they decompose rapidly into free electrons and atoms; through further impact the atoms are ionized into electrons and positive ions. These considerations are only speculative, but they could yield a plausible explanation of the experimentally found high current densities of about 10^8 A/cm^2 and greater.

The purely ohmic part of the cathode voltage U_k above the spot, first drops steeply from relatively high values, passes through a minimum and then increases slightly. It is of interest, that the high voltages at the start are caused mainly by the high heat-conductivity losses into the electrode material at the beginning. In the first moment after the ignition of the spot discharge, the temperature decay at the phase boundary layer solid-liquid is very steep (see Fig. 8) and therefore the heat flux into the solid cathode is very high. The actual ignition is not described by this analysis. The ignition voltage however has to be surely greater than or at least equal to the purely ohmic cathode voltage U_k, calculated here, to initiate a spot discharge which leads to a craterlike cavity.

Also, the time when the channel becomes unstable is not included in this evaluation - the assumption was that the stability criterion (1) or (4) is just satisfied at any time. This means that the product of current and current density Ij would reach its maximum at the same time as the vapor pressure p_c. However, it is improbable that with a further increase of temperature, current and voltage, the emission or the average current density j at the liquid surface of the crater would decrease. An increase of

j would however lead to an immediate falling short of the stability criterion (4) and therefore cause the kinking of the discharge channel [5],[16]. As a consequence of this plausible discrepancy, we have to expect the extinction of this individual spot discharge if the vapor pressure p_c reaches its maximum. In our calculated examples this maximum lies at ca. 30 ns and at a current of 80 A for copper and at ca. 4 ns and 30 A for molybdenum.

REFERENCES

1) B. Jüttner "Beitr. Plasmaphysik" Vol. 19 p. 25 (1979)
2) A.E. Guile and B. Jüttner "IEEE Transactions on Plasma Science" Vol. PS - 8 No3 p. 259 (1980)
3) J.E. Daalder "Diss. Thesis" Univ. Eindhoven (1978)
4) J.M. Lafferty "Vacuum Arcs" John Wiley and Sons (1980)
5) M. Auweter-Ming and H.O. Schrade "J. Nucl. Materials 93 and 94" p.799 (1980)
6) H.O. Schrade,M. Auweter-Ming and H. Kurtz "Proc. XV Int. Conf. on Phen. in Ion. Gases" p. 531 (Minsk 1981)
7) J.P. Datlev, A.E. Guile, B. Jüttner "Beitr. Plasmaphys." Vol. 21, No 2, p. 135 (1980)
8) J.E. Daalder "J. Phys. D", Vol 9, p. 2379 (1977)
9) D.T. Tuma et. al. "J. Appl. Phys. 49" p. 3821 (1978)
10) Hultgren, Orv., Anderson and Kelly "Selected Values of Thermodynamic Properties and Alloys" John Wiley and Sons Inc. (1963)
11) E. Hantzsche, B. Jüttner, V.F. Puchkarov, W. Rohrbeck and H. Wolff "J. Phys. D." Vol. 9, p. 1771 (1976)
12) G. Ecker "Ergebnisse d. exakten Naturwiss. 23" (1961)
13) G.N. Fursey "Local Elementary Processes at the Formation and Operation of Vacuum Arcs"*)
14) R. Clampitt and D.K. Jefferies "Proc. of the third Int. Conf. on Ion Beam Analysis" Washington, D.C. (1977)
15) J. Mitterauer "Liquid Metal Field Ion and Electron sources"*)
16) H.O. Schrade, M. Auweter-Ming and H.L. Kurtz "Analysis of the Nonstationary Low Pressure Arc Cathode Proc. VIIth Int. Conf. on Gasdischarges and their Applications" London (Sept. 1982)
17) L.D. Landau, E.M. Lifschitz "Lehrbuch der theoret. Physik VI; Hydrodynamik" Akademie Verlag Berlin p. 230 (1966)

*) presented at the Vth Workshop on Electrode Phen. Berlin 1982; organized by Zentralinstitut für Elektronenphysik, Academy of Science of GDR

APPENDIX A

Before solving the heat flow problem as demonstrated in Fig. 7, the following problem must be considered:
During $t<0$, the temperature within the homogeneous medium surrounding a sphere with radius r_{so} is set to be T_∞. At $t = 0$, the temperature at the surface of the sphere jumps suddenly from T_∞ to $T_o = T_s$ and for $t>0$ it increases steadily, corresponding to $T_o(t \geq 0) = T_s + \Delta T_{so}(t)$. Beginning with $t = 0$, a homogeneous, radial current flows through the outer medium, which leads to additional ohmic heat sources. The heat flow equation describing the time dependent spacial temperature behavior is given by

$$\frac{\partial T}{\partial t} = \frac{\chi}{r^2} \frac{\partial}{\partial r}\left(r^2 \frac{\partial}{\partial r} T\right) + \beta_J \cdot^2 \qquad \text{(A1)}$$

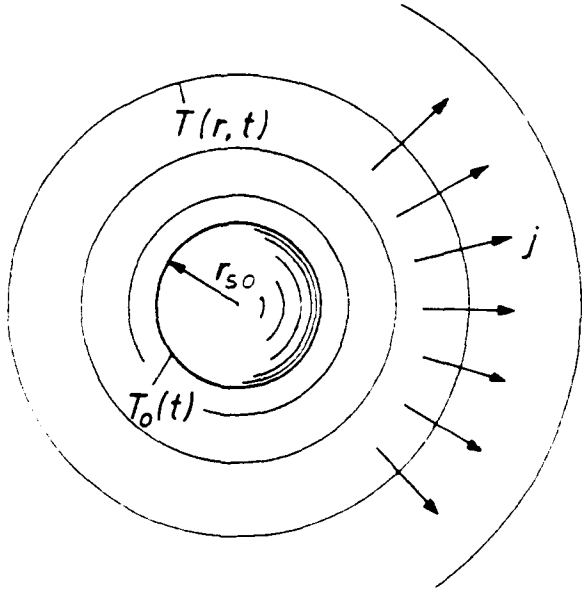

Fig. A1: Temperature distribution around a ball with the surface temperature T_s.

with the conditions:

$$T(r_{s_0}, t) = \bar{T}_0(t) = \begin{cases} \bar{T}_\infty & \text{for } t < 0 \\ \bar{T}_S + \Delta\bar{T}_{s_0} & \text{for } t \geq 0 \end{cases}$$

$$T(r \to \infty; t) = \bar{T}_\infty = \text{const.}$$

Solution:

- The term βj^2 with $j = \frac{I}{2\pi r^2}$ is represented within each hemispherical shell by the potential function

$$\beta j^2 \sim \varphi \tag{A2}$$

- Substitution:
$$T(r,t) = T^*(r,t) + \int_0^t \beta j^2 dt \tag{A3}$$

Since now

$$\Delta(\beta j^2) = \frac{1}{r^2}\frac{\partial}{\partial r}\left[r^2 \frac{\partial}{\partial r}(\beta j^2)\right] \sim \Delta\varphi = 0$$

the heat conduction equation becomes

$$\frac{\partial}{\partial t} T^*(r,t) = \frac{\chi}{r^2}\frac{\partial}{\partial r}\left(r^2 \frac{\partial}{\partial r} T^*(r,t)\right) \tag{A4}$$

within the time interval the conditions are

$-\infty < t < 0$ $\quad T^*(r,t) = T(r,t) - \bar{T}_\infty$ für alle r

$0 \leq t < +\infty$ $\quad T^*(r_{s_0}, t) = T_S + \Delta T_{s_0}(t)$

with $T_S^* = T_S - \int_0^t \beta j^2 dt$

$T^*(r \to \infty; t) = T_\infty^* = \bar{T}_\infty$

The solution of this problem is found with Landau-Lifschitz 17) as

$$\bar{T}^*(r,t) - \bar{T}_\infty^* = \frac{r_{s0}\,(r-r_{s0})}{2r\sqrt{\pi\chi}} \int_{\tau=-\infty}^{t} \frac{\bar{T}^*(r_{s0},\tau) - \bar{T}_\infty^*}{(t-\tau)^{3/2}}\, e^{-\frac{(r-r_{s0})^2}{4\chi(t-\tau)}}\, d\tau \qquad \text{(A5)}$$

where

$$\bar{T}^*(r_{s0},\tau) - \bar{T}_\infty^* = \begin{cases} 0 & \text{für } \tau < 0 \\ T_S - \bar{T}_\infty + \Delta T_{s0}(\tau) - \int_0^\tau \beta_j^{\cdot 2}(r_s)\, dt & \text{für } \tau \geq 0 \end{cases}$$

With this approach the temperature field is determined if the temperature $T^*(r_{s0},\tau)$ on the surface of the sphere is known at any time. The location of the temperature front, T_S, at any time is known by experiment. Therefore we try to reduce the time dependent temperature behavior on the surface of the sphere to the behavior of the temperature front T_S.

Choosing

$$f(\tau) = \frac{\Delta\bar{T}_{s0}(\tau) - \int_0^\tau \beta_j^{\cdot 2}(r_s,t)\, dt}{\bar{T}_S - \bar{T}_\infty} \qquad \text{(A6)}$$

the solution with

$$x = \frac{r-r_{s0}}{2\sqrt{\chi t}} \qquad \text{(A7)}$$

results in

$$\bar{T}(r,t) - \bar{T}_\infty = \frac{r_{s0}}{r}\left(\bar{T}_S - \bar{T}_\infty\right)\left\{1 - \Phi(x) + \frac{1}{\pi}\, x\sqrt{t} \int_{\tau=0}^{t} \frac{f(\tau)}{(t-\tau)^{3/2}}\, e^{-\frac{(r-r_{s0})^2}{4\chi(t-\tau)}}\, d\tau \right.$$
$$\left. + \int_0^t \beta_j^{\cdot 2}(r,t)\, dt \right. \qquad \text{(A8)}$$

where $\Phi(x) = \frac{2}{\sqrt{\pi}} \int_0^x e^{-\gamma^2} d\gamma$ is the error function.

With the substitution

$$\gamma = \frac{r - r_{s_0}}{2\sqrt{\chi(t-\tau)}} \quad , \quad d\gamma = \frac{r - r_{s_0}}{4\sqrt{\chi}\,(t-\tau)^{3/2}}\, d\tau \qquad (A9)$$

and using (A7)

$$\tau = \tau(\gamma) = t\left(1 - \frac{x^2}{\gamma^2}\right) \qquad (A10)$$

the following solution is obtained:

$$T(r,t) - \bar{T}_\infty = \frac{r_{s_0}}{r}\left(\bar{T}_s - \bar{T}_\infty\right)\left\{1 - \Phi(x) + \frac{2}{\sqrt{\pi}} \int_x^\infty f(\tau)\, e^{-\gamma^2} d\gamma\right\} + \int_0^t \beta j^2(r,t)\, dt \qquad (A11)$$

As can be shown analytically with the linear approach

$$f(\tau) = f(\tau = 0) + \left(\frac{\partial f}{\partial \tau}\right)_{\tau=0} \tau \qquad (A12)$$

(A8) or (A11) are the solutions of the problem. In the same way, at any time $\tau = \tau_0 + \Delta\tau$ ($\Delta\tau$ small), the function $f(\tau)$ can be approached with

$$f(\tau) = f(\tau_0) + \left(\frac{\partial f}{\partial \tau}\right)_{\tau_0} (\tau - \tau_0) \qquad (A13)$$

This yields also the equation (A8) or (A11).

Substituting f(τ) in Eq. A(11) with respect to A(13) we obtain

$$T(r,t) - \bar{T}_\infty = \frac{r_0}{r}\left(\bar{T}_s - \bar{T}_\infty\right)\left\{1 - \phi(x) + \frac{2}{\sqrt{\pi}}\int_x^\infty \left\{\left[f(\tau_0) - \left(\frac{\partial f}{\partial \tau}\right)_{\tau_0}\tau_0\right] + \left(\frac{\partial f}{\partial \tau}\right)_{\tau_0}\tau\right\} e^{-\gamma^2} d\gamma + \int_0^t \beta_j^{\,2}(r,t)\, dt \right. \tag{A14}$$

or by using $$f(\tau_0) - \left(\frac{\partial f}{\partial \tau}\right)_{\tau_0}\tau_0 \equiv k_0(\tau_0)$$

and calculating $\bar{T}(r,t)$ with (A10)

$$T(r,t) - T_\infty = \frac{r_0}{r}\left(\bar{T}_s - \bar{T}_\infty\right)\left\{\left[1 - \phi(x)\right]\cdot\left[1 + k_0\right] + \left(\frac{\partial f}{\partial \tau}\right)_{\tau_0} t\ \delta(x)\right\} + \int_0^t \beta_j^{\,2}(r,t)\, dt \tag{A15}$$

where

$$\delta(x) = \frac{2}{\sqrt{\pi}}\int_x^\infty \left(1 - \frac{x^2}{\gamma^2}\right) e^{-\gamma^2} d\gamma = \left[1 - \phi(x)\right](1 + 2x^2) - \frac{2}{\sqrt{\pi}}\, x\, e^{-x^2} \tag{A16}$$

and $$x = \frac{r - r_0}{2\sqrt{\chi t}}$$

k_0 and $\left(\frac{\partial f}{\partial \tau}\right)_{\tau_0}$ have to be chosen at any time with respect to the condition that the location of the temperature front at time t in the surrounding medium is the experimentally given one. So we obtain from

$$T(r,t)\Big|_{r=r_s(t)} = \bar{T}_s = \text{const.}$$

and with (A15):

$$\bar{T}_s - \bar{T}_\infty = \frac{r_0}{r_s}(T_s - \bar{T}_\infty)\left\{\left[1-\phi(x_s)\right]\left[1+k_0\right] + \left(\frac{\partial f}{\partial \tau}\right)_{\tau_0} t\,\delta(x_s)\right\} + \int_0^t \beta_j^{\,2}(r_i,t)\,dt \tag{A17}$$

with $$x_s = \frac{r_s - r_{s0}}{2\sqrt{\chi t}} \tag{A18}$$

Following from (A17), because of $t \to 0$, $r_s = r_{s0}$, and $x_s \to 0$,

$$1 = \frac{r_{s0}}{r_{s0}}\left\{\left[1-0\right]\left[1+k_0\right]+0\right\}+0$$

that is,

$$k_0 = 0 \tag{A19}$$

In the same way we obtain with (A17) and (A19)

$$t\cdot\left(\frac{\partial f}{\partial \tau}\right)_{\tau_0} = \frac{1}{\delta(x_s)}\left\{\frac{r_s(t)}{r_{s0}}\left[1-\frac{\int_0^t \beta_j^{\,2}(r_i,t)\,dt}{\bar{T}_s-\bar{T}_\infty}\right]\left[1-\phi(x_s)\right]\right\} \tag{A20}$$

Using this together with (A19), Eq. (A15) yields the temperature distribution, at any time, and at any place

$$T(r,t)-\bar{T}_\infty = \frac{r_{s0}}{r}(T_s-\bar{T}_\infty)\left\{\left[1-\phi(x)\right]-\frac{\delta(x)}{\delta(x_s)}\left[1-\phi(x_s)\right] + \frac{\delta(x)}{\delta(x_s)}\,\frac{r_s(t)}{r_{s0}}\left[1-\frac{\int_0^t \beta_j^{\,2}(r_s,t)\,dt}{T_s-\bar{T}_\infty}\right]\right\} + \int_0^t \beta_j^{\,2}(r,t)\,dt \tag{A21}$$

where

$$x = \frac{r - r_{s0}}{2\sqrt{\chi t}} \quad ; \qquad x_s = \frac{r_s - r_{s0}}{2\sqrt{\chi t}}$$

$$\delta(x) = \left[1 - \phi(x)\right](1 + 2x^2) - \frac{2}{\sqrt{\pi}} \times e^{-x^2}$$

$$\phi(x) = \frac{2}{\sqrt{\pi}} \int_0^x e^{-y^2} dy$$

APPENDIX B

Calculation of the heat flow $2\pi r_s^2 \dot{q}_f$

The heat flow at time t through the surface of a half sphere with radius $r(>r_s)$ into the colder solid body leads to

$$2\pi r^2 \dot{q}_f(r,t) = -2\pi r^2 \lambda_f \frac{\partial}{\partial r} T(r,t) \qquad (B1)$$

The heat flow is obtained as a function of t with the passage to the limit:

$$2\pi r_s^2 \dot{q}_f(t) = 2\pi r^2 \dot{q}_f(r,t)\Big|_{r\to r_s} = -2\pi r_s^2 \lambda_f \frac{\partial}{\partial r} T(r,t)\Big|_{r\to r_s} \qquad (B2)$$

$\frac{\partial}{\partial r} T(r,t)$ can be calculated with Eq. (A21):

$$\frac{\partial}{\partial r} T(r,t) = -\frac{r_{s0}}{r^2}(\bar{T}_s - \bar{T}_\infty)\left\{1 - \Phi(x) + \frac{\delta(x)}{\delta(x_s)}[\ldots.]\right\} + \frac{r_{s0}}{r}(\bar{T}_s - \bar{T}_\infty)$$
$$\cdot\left\{-\frac{2}{\sqrt{\pi}} e^{-x^2} + \frac{\frac{\partial}{\partial x}\delta(x)}{\delta(x_s)}[\ldots.]\right\}\frac{1}{2\sqrt{\kappa t}} + \frac{\partial}{\partial r}\int_0^t \beta_j^2(r)\,dt$$

with
$$\frac{\partial \delta(x)}{\partial x} = -\frac{2}{\sqrt{\pi}} e^{-x^2}(1-2x^2) + [1-\Phi(x)]\,4x - \frac{2}{\sqrt{\pi}} e^{-x^2} + \frac{4}{\sqrt{\pi}} x^2 e^{-x^2}$$
$$= 4x[1-\Phi(x)] - \frac{4}{\sqrt{\pi}} e^{-x^2} .$$

In addition is

$$\frac{\partial}{\partial r}\int_0^t \beta_j^2\,dt = \int_0^t \frac{\partial}{\partial r}\varphi\,dt = -\int_0^t \frac{1}{r}\varphi\,dt \approx -\frac{1}{r}\int_0^t \beta_j^2\,dt$$

because of $\varphi \sim \frac{1}{r}$ (potential function) and therefore

$$\frac{\partial}{\partial r} T(r,t) = -\frac{r_{s0}}{r^2}(T_s - T_\infty)\left\{1 - \phi(x) + \frac{\delta(x)}{\delta(x_s)}[\dots]\right\} + \frac{1}{2\sqrt{\pi t}}\frac{r_{s0}}{r}(T_s - T_\infty)$$

$$\cdot\left\{-\frac{2}{\sqrt{\pi}}e^{-x^2} - \frac{\frac{4}{\sqrt{\pi}}e^{-x^2} - 4x[1-\phi(x)]}{\delta(x_s)}[\dots]\right\} - \frac{1}{r}\int_0^t \beta_j^{\,2}\,dt$$

with $$[\dots] = \left[\frac{r_s}{r_{s0}}\left(1 - \frac{\int_0^t \beta_j^{\,2}(r_s)\,dt}{T_s - T_\infty}\right) - [1-\phi(x)]\right]$$

for $r \to r_s \rightsquigarrow x \to x_s$ results in

$$\frac{\partial}{\partial r} T(r,t)\Big|_{r\to r_s} = -\frac{r_{s0}}{r_s^2}(T_s - T_\infty)\left\{\frac{r_s}{r_{s0}}\left(1 - \frac{\int_0^t \beta_{js}^{\,2}\,dt}{T_s - T_\infty}\right)\right\} + \frac{1}{2\sqrt{\pi t}}\frac{r_{s0}}{r_s}(T_s - T_\infty)$$

$$\cdot\left\{-\frac{2}{\sqrt{\pi}}e^{-x_s^2} - \frac{\frac{4}{\sqrt{\pi}}e^{-x_s^2} - 4x_s[1-\phi(x_s)]}{\delta(x_s)}[\dots]\right\} - \frac{1}{r_s}\int_0^t \beta_{js}^{\,2}\,dt$$

$$= -\frac{1}{r_s}(T_s - T_\infty) + \frac{r_{s0}}{r_s(r_s - r_{s0})}(T_s - T_\infty)\left\{-\frac{2}{\sqrt{\pi}}x_s e^{-x_s^2}\right.$$

$$-\frac{2}{\delta(x_s)}\left(\frac{2}{\sqrt{\pi}}x_s e^{-x_s^2} - 2x_s^2[1-\phi(x_s)]\right)\left[\frac{r_s}{r_{s0}}\left(1 - \frac{\int_0^t \beta_{js}^{\,2}\,dt}{T_s - T_\infty}\right)\right.$$

$$\left.\left. - [1-\phi(x_s)]\right]\right\} + \frac{2}{\delta(x_s)}\left(\delta(x_s) - [1-\phi(x_s)]\right)$$

$$\frac{\partial}{\partial r} T(r,t)\Big|_{r\to r_s} = -\frac{1}{r_s}(T_s - T_\infty)\left\{1 + \frac{r_{s0}}{r_s - r_{s0}}\left[\frac{2}{\sqrt{\pi}}x_s e^{-x_s^2} + 2\left(\frac{1-\phi(x_s)}{\delta(x_s)} - 1\right)\right.\right.$$

$$\left.\left.\cdot\left[\frac{r_s}{r_{s0}}\left(1 - \frac{\int \beta_{js}^{\,2}\,dt}{T_s - T_\infty}\right) - 1 + \phi(x_s)\right]\right]\right\} =$$

$$= -\frac{1}{r_s}(T_s-T_\infty)\left\{1+\frac{2}{\sqrt{\pi}}x_0 e^{-x_s^2}+2\left(\frac{1-\phi(x_s)}{\delta(x_s)}-1\right)\right.$$

$$\left.\cdot\left[1-\frac{r_s}{r_s-r_{s0}}\,\frac{\int_0^t \beta_{js}^2\,dt}{T_s-T_\infty}+\frac{r_{s0}}{r_s-r_{s0}}\,\phi(x_s)\right]\right\}$$

$$= -\frac{1}{r_s}(T_s-T_\infty)\left\{1+\frac{1}{\sqrt{\pi x t}}e^{-x_s^2}-\frac{2}{\sqrt{\pi}}x_s e^{-x_s^2}\right.$$

$$\left.+2\left(\frac{1-\phi(x_s)}{\delta(x_s)}-1\right)\left[1+\frac{r_{s0}}{r_s-r_{s0}}\,\phi(x_s)-\frac{r_s}{r_s-r_{s0}}\,\frac{\int_0^t \beta_{js}^2\,dt}{T_s-T_\infty}\right]\right\}$$

$$\frac{\partial}{\partial r}T(r,t)\Big|_{r\to r_s} = -\frac{1}{r_s}(T_s-T_\infty)\left\{1+\overbrace{\frac{r_s}{\sqrt{\pi x t}}-\frac{2}{\sqrt{\pi}}x_s}^{=0}-\frac{2}{\sqrt{\pi}}x_0+\frac{2}{\sqrt{\pi}}x_0 e^{-x_s^2}\right.$$

$$\left.+2\left(\frac{1-\phi(x_s)}{\delta(x_s)}-1\right)\left[1+\frac{x_0}{x_s}\,\phi(x_s)-\frac{x_0}{x_s}\,\frac{r_s}{r_{s0}}\,\frac{\int_0^t \beta_{js}^2\,dt}{T_s-T_\infty}\right]\right\}$$

Therefore the heat flow follows as

$$2\pi r_s^2 \dot{q}_f(t) = 2\pi\lambda_f r_s (T_s-T_\infty)\left\{1+\frac{2}{\sqrt{\pi}}x_0 e^{-x_s^2}+2\left(\frac{1-\phi(x_s)}{\delta(x_s)}-1\right)\right.$$

$$\left.\cdot\left[1+\frac{x_0}{x_s}\left(\phi(x_s)-\frac{r_s}{r_{s0}}\,\frac{\int_0^t \beta_{js}^2\,dt}{T_s-T_\infty}\right)\right]\right\} \qquad \text{(B3)}$$

END

FILMED

2-85

DTIC